The balance between intrinsic and ecological fitness defines new regimes in eco-evolutionary population dynamics

Rowan J. Barker-Clarke[1], Jason M. Gray[1,2], Maximilian A. R. Strobl[1], Jeff Maltas[1,3], Dagim Shiferaw Tadele[1,4], Michael Hinczewski[2,†], and Jacob G. Scott[1,2,5,†]

[1]Translational Hematology & Oncology Research, Cleveland Clinic, Cleveland OH, 44106, USA
[2]Department of Physics, Case Western Reserve University, Cleveland, OH, 44106, USA
[3]Case Western Reserve University Department of Genetics, Cleveland, OH, 44106, USA
[4]Oslo University Hospital, Ullevål, Department of Medical Genetics, Oslo, Norway.
[5]Case Western Reserve University School of Medicine, Cleveland, OH, 44106, USA
[†]michael.hinczewski@case.edu, scottj10@ccf.org

ABSTRACT

Selection upon intrinsic fitness differences is one of the most basic mechanisms of evolution, fundamental to all biology. Equally, within macroscopic populations and microscopic environments, ecological interactions influence evolution. Direct experimental evidence of ecological selection between microscopic agents continues to grow. Whilst eco-evolutionary dynamics describes how interactions influence population fitness and composition, we build a model that allows ecological aspects of these interactions to fall on a spectrum independent of the intrinsic fitness of the population. With our mathematical framework, we show how ecological interactions between mutating populations modify the estimated evolutionary trajectories expected from monoculture fitnesses alone. We derive and validate analytical stationary solutions to our partial differential equations that depend on intrinsic and ecological terms, and mutation rates. We determine cases in which these interactions modify evolution in such ways as to, for example, maintain or invert existing monoculture fitness differences. This work discusses the importance of understanding ecological and intrinsic selection effects to avoid misleading conclusions from experiments and defines new ways to assess this balance from experimental results. Using published experimental data, we also show evidence that real microbiological systems can span intrinsic fitness dominant and ecological-effect dominant regimes and that ecological contributions can change with an environment to exaggerate or counteract the composite populations' intrinsic fitness differences.

Conflict of Interest Statement: The authors have no conflicts of interest to disclose.

Introduction

Across biology, evolutionary selection pressure acts upon phenotypes and, when sufficiently strong, can alter the genotype of an entire population over successive generations. Without interactions between populations, each phenotypic fitness is defined entirely by the genome and epigenome, in combination with the external evolutionary pressure of the environment, whether that takes the form of drug, temperature, or other factors. [1] In this regard, the genetic fitness landscape has been a key concept for understanding cell-intrinsic fitness, selection, and evolution.

Fitness landscapes map out the fitness or reproductive potential of an individual based on its location in an abstract genotype space. Peaks in this landscape correspond to high-fitness regions, where dynamics are dominated by natural selection, while flat regions promote diffusive neutral evolution (drift), resulting in increased evolutionary stochasticity. [2] Under these non-ecological assumptions, the trajectory of evolution for a mutating population is predicted based upon the mutational supply to a population and the relative fitness of each of these genotypic populations in monoculture, i.e. treating the genotype as if it was growing in isolation from all other genotypes. [3]

While important, individual fitness is not the only factor potentially influencing mixed population dynamics. At the opposite extreme, ecological and game theoretical modeling approaches such as the Lotka-Volterra and replicator equations are well-established descriptions of how interactions impact the long-term dynamics and stable states of mixtures of competing populations. [4–7] It is the interplay between these two approaches (genotypic evolution and ecology) that is of particular interest in the treatment of evolving, multicellular diseases like cancer and complex infections. For example, while the

heterogeneity of genotypes within a patient's disease is accepted as a driver of both pre-existing or de-novo resistance evolution, the presence of cell-cell interactions in this mixed population may further contribute to altering the efficacy of drugs. It is often the case that personalized treatment in evolving diseases eventually encounters resistance, the reasons for which likely include a combination of stochastic, ecological, and genotypic factors. [8, 9]

Ecological interactions can lead to frequency-dependent selection—fitness that varies with the relative fraction of a genotype in a mixed population. In recent years this phenomenon has been directly observed in disease contexts and shown to be a mechanism for maintaining diversity, particularly in bacterial systems. [10–17] Frequency-dependent selection has also been found in cancer cell lines with varying microenvironments: Kaznatcheev *et al.* [17] demonstrated how alectinib-resistant and parental non-small cell lung cancer cells have different fitnesses across relative population frequencies and how the presence of fibroblasts or changing treatment results in distinct frequency-dependent functional changes in fitness (often termed evolutionary games). Many papers have also used game theory to model tumor growth and composition, with the presence of interactions between cells including competing tumor and stromal cells and the production of growth factors as a strategy. [18–24] Theoretical studies have also shown the potential of frequency-dependent selection to promote high mutation rates and accelerate evolution. [25, 26]

Given the increasing experimental evidence and theoretical interest in game interactions, it is notable that the overwhelming majority of assays in experimental evolution still measure the fitness of genotypes in monoculture. In the present work, we argue that if these results are used to predict coculture behavior, there is a significant risk of making misleading conclusions, since the existence of game interactions can readily modify evolutionary outcomes in ways that contradict the expectations resulting from monoculture data. [26] **Figure 1** schematically illustrates the extent of potential difficulties by introducing four hypothetical ways in which ecological interactions could change outcomes, and how these outcomes agree or disagree with expectations based on monoculture results. Consider two genotypes in each row, labeled by different colors in the figure (red and blue). The fitness landscapes show the monoculture fitness of each on the y-axis, where red has higher monoculture fitness in each row except the last where the blue and red have equal fitnesses. The first scenario, which we call *maintenance*, occurs when the interactions are present but rendered effectively invisible: a co-cultured mixture of two types will behave exactly as expected from monoculture, for example with red eventually out-competing blue. This could be due to the absence of interactions, but as we will show below there is also a set of non-zero interaction strengths that lead to maintenance. The second scenario is *masking*: two genotypes behave as if equally fit (neutral) when co-cultured, despite monoculture fitness differences. The third scenario is *mirroring*: where one is expected to dominate based on monoculture fitness (i.e. red versus blue) but the result is perfectly inverted and blue outcompetes red to the same degree. The final scenario is *mimicry*: if two genotypes have equal monoculture fitness but effectively behave as if one has a selective advantage when co-cultured. This is not an exclusive list of possibilities and indeed most interactions strengths will lead to behaviors that mix different aspects of these cases. We focus on these four scenarios because they present interesting examples that clearly illustrate the potential confounding effects of ecology; interactions can be present even if a net effect is absent, and switching between monoculture and co-culture can either exacerbate or mitigate selective differences.

Our work expands upon multiple works that have formalized the frequency-dependent Wright-Fisher model in several dimensions [27–29] and prior co-evolutionary dynamic descriptions. [30–32] An underlying assumption of many of these models, including ours, is that the strategy of a cell is set by its genotype and therefore by its parent. Under this assumption, the "payoff" of the evolutionary game is reflected in a cell's ability to replicate, i.e. producing another player of the same type. We develop an expanded game-theoretic formalism that is biologically motivated in light of growing experimental assays and evidence and decomposes cell-intrinsic and cell-extrinsic interactions. This allows the study in both deterministic and stochastic settings of variable relative interaction strengths in biological replicator populations with intrinsic growth rate differences. Using a stochastic, agent-based model, we simulate a frequency-dependent Wright-Fisher model in 1-dimension. We find stationary solutions to the Fokker-Planck equation that allow us to formally compare evolutionarily stable states between deterministic and stochastic games. We derive and validate expressions for the conditions on the game interactions in the 1-dimensional case that cause the resultant evolution to perfectly maintain, mimic, mirror, or mask the dynamics of an initial genetic fitness landscape. Such a hypothesis concludes that if ecological factors and interactions can readily change evolutionary outcomes so dramatically, the evolution of the population should be modeled using game theory and population genetics in tandem. Our work emphasizes that knowledge of cell-extrinsic interaction strengths is essential in accurately predicting and interpreting evolution in co-culture. To examine the potential frequency of these regimes in real biological systems we analyzed several published experimental results. Through our transformation of variables, we show the comparative contributions of ecology and intrinsic selection in these different reported systems. Using numerical methods we also estimate the proximity of these systems to the theoretical regimes of maintenance, masking, and mirroring.

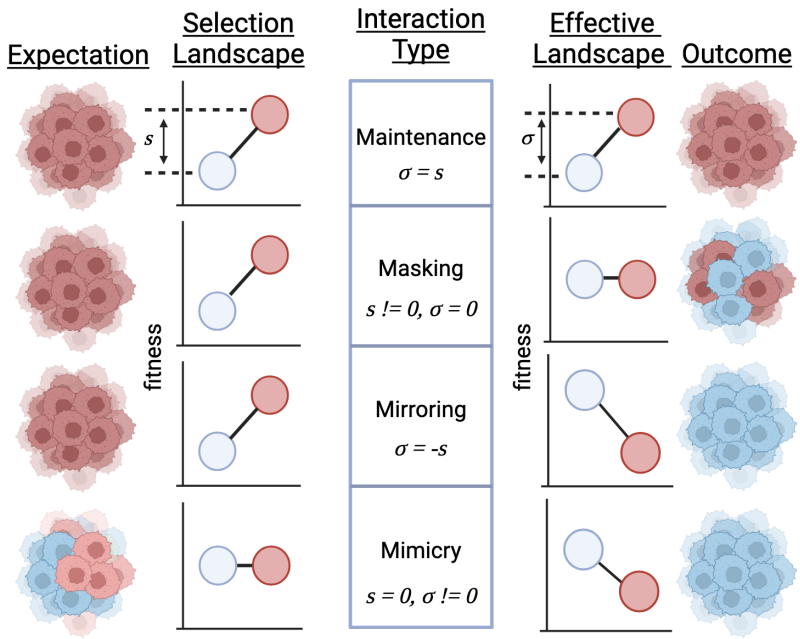

Figure 1. What are maintenance, masking, mirroring, and mimicry? Based upon the monoculture fitness landscape of different cell types (left, with the different fitness landscapes each representing two genotypes and their intrinsic fitness), there is a baseline expectation of how the evolutionary dynamics of a mixed population (blue and red) would play out. This is without interactions based upon the intrinsic selection difference s. This expectation is shown in the second column. For co-cultured populations, interactions can modify the fitnesses and result in different evolutionary dynamics in co-culture. The effective fitness landscape has a selection difference of σ. For example, if red has a higher fitness in the fitness landscape, the resultant dynamics should be dominated by red. The actual results are modified by interactions, and the four rows show four representative ways in which interactions confound monoculture expectations: maintenance, masking, mirroring, and mimicry, discussed in more detail in the text.

Theory and Results

To develop our theoretical approach, we start with a simple model of evolutionary game dynamics in the absence of noise and mutation. Game theory in general is the study of the dynamics which result from the interaction of different strategies played against each other. Specific strategies result in expected payoffs for the players and thus the average payoff depends upon the frequency of strategies in the system. Differential game theory can describe deterministic solutions for these dynamics using differential equations. In a symmetric game, the time ordering of the played strategy does not affect the payoffs for the players involved. The payoffs in a 2-strategy symmetric differential game can be presented as a payoff matrix in the following way [7, 33]:

$$P = \begin{pmatrix} a & b \\ c & d \end{pmatrix}, \tag{1}$$

where a is the payoff for a player with strategy 1 playing against another player of type 1, b is the payoff for a player with strategy 1 playing against a player of type 2, c is the payoff for a player with strategy 2 playing against a player of type 1, and d is the payoff for a player with strategy 2 playing against a player of type 2. These values determine the expected payoffs or "fitnesses" for each player when the frequencies of strategies in the population are known.

For our model, available "strategies" are the cell types of the populations under study. In the replicator model, a cell cannot actively choose a strategy, because the cell's strategy (phenotype) and identity (genotype) form a one-to-one mapping. Under the assumption that a cell's genome determines its strategy, we use a simplified model comprising a single locus with two alleles, the wild-type and the mutant, the latter harboring a resistance mutation at the site of interest. In genetic population models, strategy proportions change when cells undergo self-replication, with fitter strategies reproducing at a faster rate. In this type of model, the cells are called replicators: players with strategies that are determined by the strategy of their parent.

The underlying assumption of replicator dynamics is that the fitness of a cell with strategy i is proportional to the difference between the fitness of its strategy and the average. This determines its rate of replication and this formalism and accompanying equations are referred to as replicator dynamics. [6, 33] In the 2-dimensional case with payoff matrix P from Eq. (1), the

replicator equation takes the following form:

$$\frac{\partial x}{\partial t} = x(1-x)((c-a)(1-x)-(b-d)x), \tag{2}$$

where the proportion of type 2 (mutant) is x, and thus the proportion of type 1 (wild type) is $1-x$. Without the addition of noise, the replicator equation gives us deterministic solutions for the evolutionarily stable strategies present. [34] Without mutation in the population, this equation has stationary solutions at $x=0$, $x=1$, and $x=(c-a)/((b-d)+(c-a))$. Following this, different conditions on a, b, c, and d result in various evolutionarily stable solutions. These different conditions are often labeled as different types of games (Prisoner's Dilemma, Snow Drift, Stag Hunt, and Harmony). One can construct the 2-dimensional "game space", which has the axes $c-a$ and $b-d$ as shown in **Figure 2**. A specific two player game payoff matrix has a position in one of these quadrants that categorizes it into a certain universality class. Games in the same quadrant generate similar dynamics. In the top left $c>a$ and $d>b$, the wild-type always outgrows the mutant. In the bottom right the converse is true. In the top right, $c>a$ but $b>d$, so the species co-exist. In the bottom left $c<a$ and $b<d$ such that there is an unstable mixed equilibrium that cannot persist within a stochastic system.

Cell-intrinsic and cell-extrinsic components can be logically separated within the payoff matrix

In the payoff matrix for two distinct cell populations undergoing replicator dynamics, the diagonal terms, a and d from Eq. (1) can be understood as the intrinsic monoculture growth rates of each population. The off-diagonal elements reflect the growth rate of the population in the presence of the other cell type. We model this as the population's intrinsic growth rate modified by extrinsic cell-cell interactions. To illustrate this clearly, we can represent and decompose the payoff matrix as follows:

$$\begin{aligned} P &= \begin{pmatrix} g_w & g_w+\beta_{wm} \\ g_m+\beta_{mw} & g_m \end{pmatrix} \\ &\equiv g_w \begin{pmatrix} 1 & 1+\alpha_{wm} \\ 1+s_m+\alpha_{mw} & 1+s_m \end{pmatrix} \\ &\overset{g_w\to 1}{=} \begin{pmatrix} 1 & 1+\alpha_{wm} \\ 1+s_m+\alpha_{mw} & 1+s_m \end{pmatrix} \end{aligned} \tag{3}$$

Here $g_w(=a)$ and $g_m(=d)$ are the growth rates of the wild-type and mutant cells respectively, β_{wm} is the perturbation to the wild-type growth rate due to the mutant population, and β_{mw} the perturbation to the mutant growth rate due the wild type population. In the third line, we have normalized all terms relative to the wild-type growth rate, defining the mutant selection coefficient $s_m = g_m/g_w - 1$ and two interaction coefficients $\alpha_{wm} = \beta_{wm}/g_w$, $\alpha_{mw} = \beta_{mw}/g_w$. When there are no cell-extrinsic interaction terms ($\alpha_{wm},\ \alpha_{mw} \to 0$), all entries within each row of the payoff matrix become equal. Additionally, when analyzing these dynamics we set the growth rate of the wild-type (g_w) to 1. As such there is no explicit time dependence in the resulting dynamics. After this variable transformation the replicator equation, **Eq.** (2), for the mutant can be written as follows:

$$\frac{\partial x}{\partial t} = x(1-x)((\alpha_{mw}+s_m)(1-x)-(\alpha_{wm}-s_m)x). \tag{4}$$

When there are no cell-extrinsic interaction terms ($\alpha_{wm},\ \alpha_{mw} \to 0$), the frequency-independent evolutionary dynamics are recapitulated. Any relative dynamics in a 2-player system can be defined by game coefficients α_{wm}, α_{mw}, and the mutant selection coefficient s_m.

The dynamics in a two-player game are often displayed as quadrants in a 2D game space with quadrants corresponding to different dynamical outcomes (**Fig. 2A**). Our variable transformation of the payoff matrix allows us to highlight how the quadrants are regions defined by interaction strengths relative to intrinsic selection, and their analytical forms. In the intrinsic and extrinsic form of the payoff matrix, these axes correspond to $(g_m+\beta_{mw}-g_w)$ and $(g_w+\beta_{wm}-g_m)$. Here g_i is the intrinsic growth rate of type i and β_{ij} is the maximum extent to which interaction with type j affects the growth of i. In this tranformed basis we can also write these as $g_w(\alpha_{mw}-s_m)$ and $g_w(s_m+\alpha_{wm})$ where $a=g_w$ and the quadrants can be defined by conditions on α_{mw} and α_{wm} relative to the homogeneous mutant population selection coefficient s_m (**Fig. 2B**). For the novel "interaction-selection" plot (**Fig. 2C**), we can plot the selection normalized interaction coefficients (α_{ij}/s_i, α_{ji}/s_i). As we move through different values of α_{wm} and α_{mw} relative to s_m the resultant equilibrium state is modified. We highlight the unit circle in this plot as a key region where intrinsic selection differences are dominant. As might be expected, within this circle, the game dynamics of the system, dominated by intrinsic selection, will align with the quadrant representing dominance by the same population. Deterministic boundaries between the universality classes in all phase spaces occur along the lines $\alpha_{wm} = -s_m$ and $\alpha_{mw} = s_m$ For example, the cooperation quadrant (top right) is defined by $\alpha_{wm} > s_m$ and $\alpha_{mw} > -s_m$.

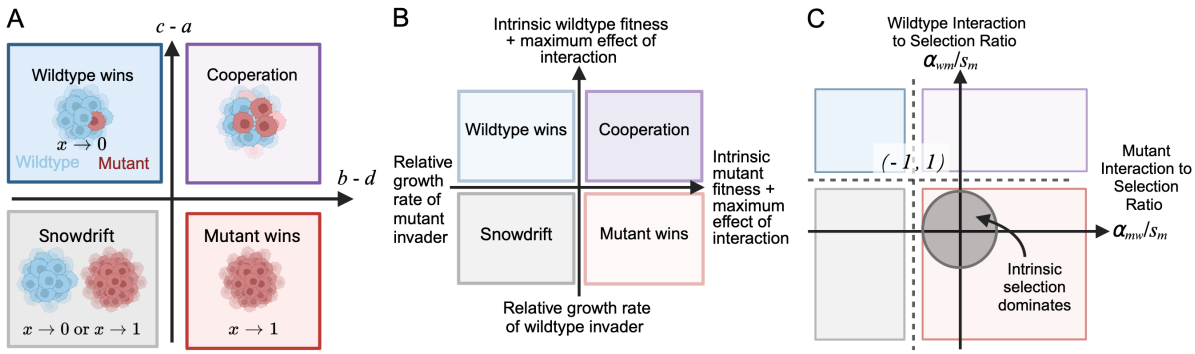

Figure 2. Resultant classes of evolutionary dynamics in the 2-player replicator game as a function of relative fitness and interaction strength. (A) Illustration of game dynamics between two populations (wild-type and mutant cells). Evolutionary game theory between two players results in four types of dynamics. In the biological case, both the cell-intrinsic and cell-extrinsic influences on growth rate come together in co-culture to produce novel dynamics. The observed dynamics rely not only on the isolated behavior of cells but also on the precise balance between intrinsic and extrinsic factors. In the top left quadrant, the wild type dominates. In the top right quadrant, a heterogeneous mixture is promoted. In the bottom right quadrant, the resistant mutant dominates. Lastly, in the bottom left quadrant, coexistence is unstable and when the population is not at this fraction, the population is driven to the nearest stable fixed point (all wild types or all mutants). **(B)** The game space reflects distinct evolutionarily stable states corresponding to the four quadrants in relative fitness space $(b-d, c-a)$. These are frequently referred to as the growth rate of an invading subspecies. In the cell-centered decoupled payoff framework, these axes are the intrinsic fitnesses and the maximum effect of interactions. **(C)** In the interaction-selection plot, a system's position is plotted as a function of interaction strengths (α_{ij}) divided by intrinsic fitness difference s. The coordinates in our mutant and wild-type system are $(\alpha_{mw}/s_m, \alpha_{wm}/s_m)$. The regions are labeled under the assumption that $s_m > 0$ and the mutant is fitter than the wild type. We highlight the unit circle in this space as the region where intrinsic selection is stronger than interaction. In this region, the fitter monoculture population (in this example the fitter population is the mutant with s_m>0) remains dominant. The color of the quadrants and position of the boundaries in this plot refers to four different universality classes within deterministic evolutionary games. Boundaries between the classes in all phase spaces occur along the lines $\alpha_{wm} = -s_m$ and $\alpha_{mw} = s_m$ and thus are mirrored accordingly in the interaction-selection plot depending on its sign.

While this variable transformation allows for evolutionary games to be framed in terms of extrinsic and intrinsic terms, the replicator dynamics above describe a deterministic system. This means that one can precisely determine the state of the system at a later time, given the state of the system at an earlier point in time. In real biological systems, genetic drift and mutation are present and both of these processes are stochastic, introducing noise into the system.

Stochastic eco-evolutionary dynamics with mutation

Given the stochastic nature of population dynamics, we use a partial differentiation equation to model the time evolution of the probability density function of a one dimensional population , the form we choose is known as the Fokker-Planck equation. [35, 36] Developed to describe the time-dependent probability distribution of a Brownian particle subject to drag forces, it has since been successfully applied in contexts that include protein folding and gene expression stability. [37–40] Its usefulness for evolution was first demonstrated by Kimura, [41] who showed that a population obeying Wright-Fisher dynamics with mutation and selection could be described via this type of reaction-diffusion equation,

$$\frac{\partial \rho(x,t)}{\partial t} = -\frac{\partial}{\partial x}\Big[v(x)\rho(x,t)\Big] + \frac{\partial^2}{\partial x^2}\Big[D(x)\rho(x,t)\Big], \tag{5}$$

where $\rho(x,t)$ is the probability density function of a population having mutant fraction x at time t. The first term on the right describes the deterministic effects of mutation and selection, which shift the peak of $\rho(x,t)$ over time, while the second term leads to a diffusive broadening of the distribution due to demographic noise (finite sampling from a population of size N). For a non-interacting system, the expressions $v(x)$ and $D(x)$ in these terms are: [41]

$$\begin{aligned} v(x) &= (1-2x)\mu + s_m g(x), \\ D(x) &= \frac{g(x)}{2N}, \end{aligned} \tag{6}$$

where μ is the mutation rate (assumed here to be symmetric for wild-type to mutant and vice versa), s_m is the mutant selection coefficient, and $g(x) = x(1-x)$.

Game-modified selection coefficient

Game dynamics between wild-type and mutant alleles result in frequency-dependent selection with a dependence on both the intrinsic growth rates of the cells and the interactions α_{wm} and α_{mw}. To modify the Fokker-Planck equation to include this

effect, we must derive a new frequency-dependent selection coefficient. To do this we find the frequency-dependent fitness of each allele using the payoff matrix in **Eq.** (3). Our payoff matrix results in the following fitness vector:

$$\begin{aligned}\vec{\phi}(\vec{x}) &= P\cdot\vec{x}\\ &= \begin{pmatrix} 1 & 1+\alpha_{wm} \\ 1+s_m+\alpha_{mw} & 1+s_m \end{pmatrix}\begin{pmatrix} 1-x \\ x \end{pmatrix}\\ &= \begin{pmatrix} 1+\alpha_{wm}x \\ 1+s_m+\alpha_{mw}(1-x) \end{pmatrix}\end{aligned} \tag{7}$$

where $\vec{x} = (1-x, x)$ is the vector of frequencies of the wild-type and the mutant. The first component of $\vec{\phi}(\vec{x}) = (\phi_w(\vec{x}), \phi_m(\vec{x}))$ is the wild-type fitness $\phi_w(\vec{x})$, and the second component is the mutant fitness $\phi_m(\vec{x})$. We thus define the interaction selection coefficient $\sigma_m(\vec{x})$ that replaces the selection coefficient s_m in the non-interacting case:

$$\begin{aligned}\sigma_m(x) &:= \frac{\phi_m(\vec{x})}{\phi_w(\vec{x})} - 1\\ &= \frac{1+s_m+\alpha_{mw}(1-x)}{1+\alpha_{wm}x} - 1\\ &= \frac{s_m+\alpha_{mw}-(\alpha_{wm}+\alpha_{mw})x}{1+\alpha_{wm}x}.\end{aligned} \tag{8}$$

We see that when there are no cell-extrinsic interaction terms ($\alpha_{wm},\ \alpha_{mw} \to 0$) this expression for the interaction selection coefficient recovers the non-interacting result, $\sigma_m(x) \to s_m$. We use this interaction selection coefficient to modify the first term in the Fokker-Planck equation, replacing the selection coefficient, s_m in $v(x)$ with the interaction selection coefficient:

$$v(x) = (1-2x)\mu + \sigma_m(x)g(x). \tag{9}$$

The diffusion term remains unchanged.

Analytical solution in terms of interaction strengths for the steady-state of the Fokker-Planck equation

A form of steady-state solution $\rho^{\text{eq}}(x)$ for the Fokker-Planck equation in **Eq.** (5) is

$$\rho^{\text{eq}}(x) = C\big[\exp\big(-U(x)\big)\big], \tag{10}$$

where C is a normalization constant, and $U(x) = \ln D(x) - \int_0^x dx'\, v(x')/D(x')$. For our interacting model the integral can be carried out explicitly, yielding

$$U(x) = (1-2N\mu)\ln(x(1-x)) - 2N\left[\frac{(1+s_m)\alpha_{wm}+(1+\alpha_{wm})\alpha_{mw}}{\alpha_{wm}^2}\ln(1+\alpha_{wm}x) - \frac{\alpha_{wm}+\alpha_{mw}}{\alpha_{wm}}x\right]. \tag{11}$$

Our solution describes a probability density distribution for a given population size, mutation rate, selection coefficient, and interaction terms. Knowledge of $\rho^{\text{eq}}(x)$ can then be used to calculate summary values of the distribution, for example, the modal mutant population fraction or the mean $\bar{x} = \int_0^1 dx' x' \rho^{\text{eq}}(x')$.

We observe (**Fig. S1**) that under very small ecological interaction and at low mutation rates, the form of the solution is similar to the deterministic case in the absence of noise, where the distributions approach delta functions at either $x = 0$ or $x = 1$. The values of both α_{mw} and α_{wm} and μN alter the width of the peaks in the probability distributions.

Stochastic simulations match stationary Fokker-Planck solution under varying independent selection and interaction strengths

To validate this Fokker-Planck solution we simulate genetic populations undergoing mutation and selection with interactions and noise using a modified Wright-Fisher model. For further simulation details see methods. The mean value of the simulation fractions is plotted in **Figure 3** for a specific $s_m (= 0.05)$ with varying interaction coefficients, and the corresponding theoretical probability distributions in several cases are shown for comparison. It is worth noting that the “snowdrift" game from the lower left quadrant in traditional game space ($c < a$ and $b < d$) has two peaks in its stationary Fokker-Planck solution, and the height of these peaks becomes more uneven with distance away from the line $\alpha_{wm} = \alpha_{mw} - 2s_m$. The width of the peaks in all sections increases with mutation rate μ.

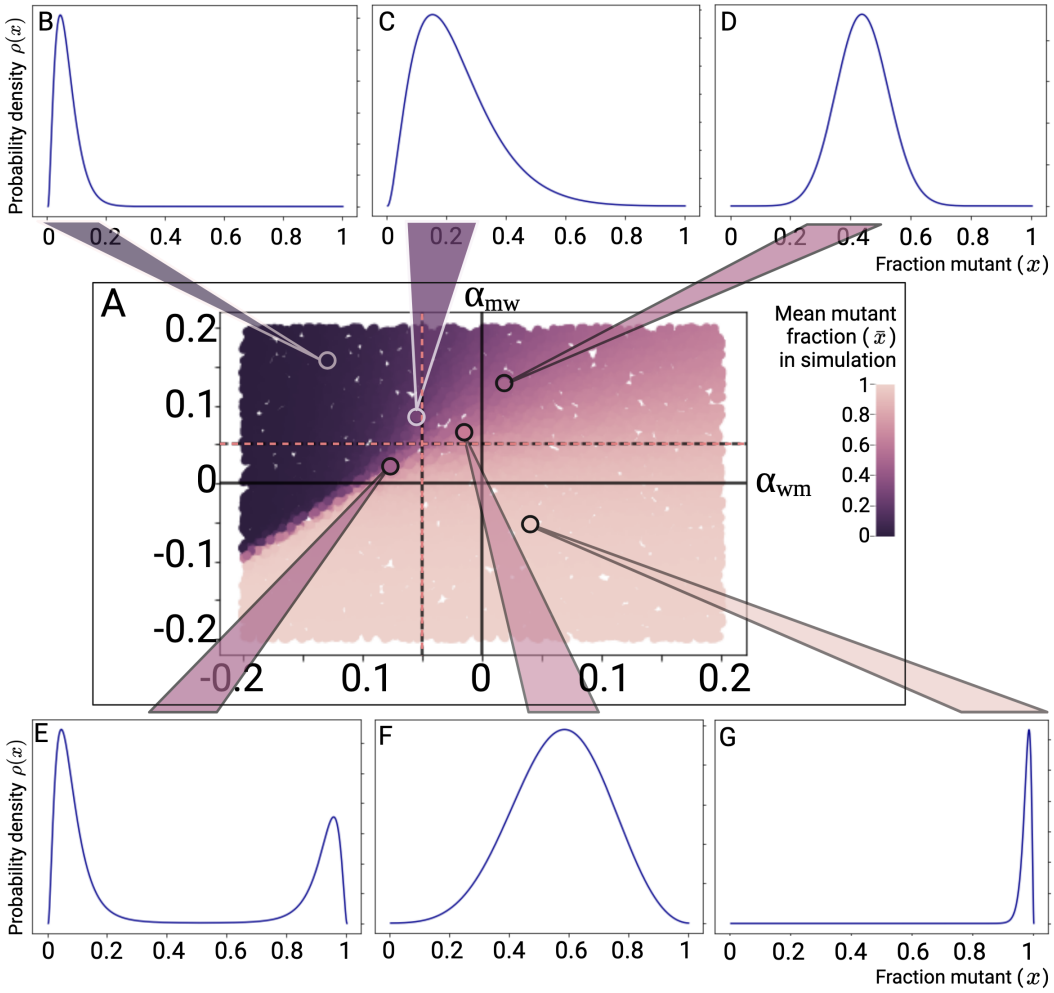

Figure 3. Simulations and equivalent Fokker-Planck solutions for examples of a stochastic evolving and mutating population. (A) The central plot displays the mean fraction of the mutant population ($\bar{x}$), plotted for 10,000 randomly distributed game parameters. Mean mutant fractions are plotted against randomly sampled interaction strengths, with mutant selection advantage $s_m = 0.05$, $N = 1000$, $\mu = 0.005$. The average (mean) proportion of mutant was plotted for each pair of interaction coefficients. Simulation results are colored by population fraction, with 100% wild-type, 0% mutant in dark purple, and 100% mutant, 0% wild-type population in cream. 10,000 random values of α_{mw}, α_{wm} in the interval $[-0.2, 0, 2]$ were sampled to populate the phase plot. Six distributed examples (**B-G**) of the analytical Fokker-Planck equilibrium solution for $\rho(x)$ against x are shown and their approximate position in the simulation space is highlighted. Distributions from the upper left and lower right (e.g., **B**, **G**) have distributions strongly peaked near 0% and 100% mutant fractions respectively. The upper right quadrant (e.g., **D**, **F**) shows stable co-existence, with solutions and simulations in the bottom left quadrant (e.g., **E**) representing probability distributions with two peaks, one at 100% wild-type and one at 0% wild-type.

In the Wright-Fisher model, with mutation and strong selection, a population will move to the peak of the landscape in a single peaked landscape, whereas in a flat landscape, fluctuates stochastically around equal proportions of all genotypes. Without interactions, the results of the Wright-Fisher model depend only on the intrinsic (genetic) fitness landscape, in particular, whether the landscape is neutral or peaked, and the mutation rate. To validate the predicted result of interactions in evolutionary simulation models we added randomly distributed interaction strengths to a Wright-Fisher model of both single-peaked ($s_m! = 0$) and flat ($s_m = 0$) landscapes.

In **Figure 4** and **Figure S1** we examine the predicted population's stationary distribution. In **Figure 4A** we plot the modal values of the analytical solution over varying for a given selection and mutation space. To validate these distributions we sampled the frequency spectrum of the population in simulations at long time points (between 100 and 10,000 generations). We compared this frequency distribution to our analytical probability density equilibrium solution for the Fokker-Planck equation with interactions. In the case of $s_m = 0$, we regain the four-quadrant game plot, representing the different classical games and their outcomes.

The equilibrium distribution of a system with known monoculture fitnesses and no game interactions is well defined and understood in population genetics. As a result, the equilibrium distributions/evolutionary outcomes measured in experiments are

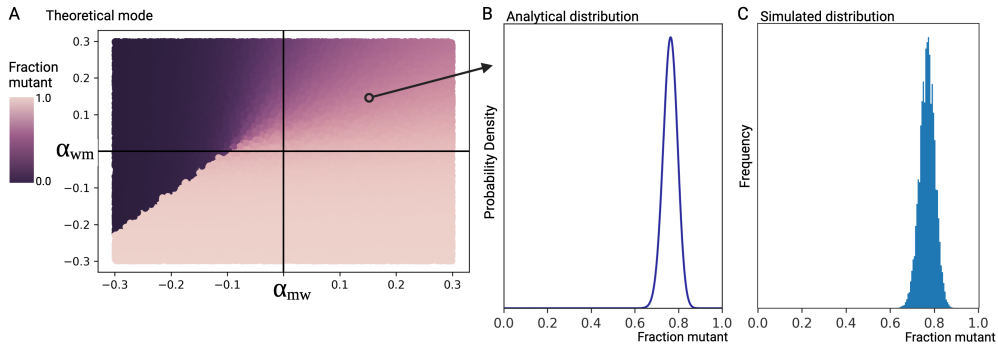

Figure 4. Fokker-Planck (FP) distribution compared to stochastic simulation results. (A) The modal value of the analytical FP distribution is plotted for 100,000 randomly generated pairs of interaction terms. Modal values of 100% wild-type are dark purple and 100% mutant fraction are colored cream. **(B)** We highlight the shape of the analytical probability density distribution in a specific Fokker-Planck solution ($\alpha_{wm} = 0.16$, $\alpha_{mw} = 0.14$, $s_m = 0.1$) and compare theoretical results in plot **(B)** to simulation. **(C)** Distribution of sampled fractions between 200 to 500 generations in 500 independent simulations is shown. These simulations had a selection coefficient of $s_m = 0.1$, representing a fitter mutant population. The histogram is a sampled distribution of the population fraction, with each sample measured at $t > 200$ generations from 500 simulations under these conditions. Further examples are shown in **Figure S2**.

often assumed to result from entirely intrinsic fitness differences. This assumption does not account for potential interactions between populations. As seen in **Figure 1**, the survival of the fittest (under which the 'fittest' genotype prevails), can result in multiple populations co-occurring and becomes population and interaction dependent.

Defining a frequency-dependent selection coefficient for the probability density distribution

To examine the specific conditions in which interactions may alter the outcomes of biological systems and experiments, we need to understand how the probability density distribution representing the relative fractions in the population shifts with different interaction strengths. This is equivalent to the dependence of the modal value of the stationary solution on the interaction terms. In particular, our concepts of maintenance, masking, mirroring, and mimicry rely on how this modal value changes compared to the mode of the probability density distribution for the system without interactions.

This modal population fraction, x_{mode}, is where the peak of the probability distribution is located. The location of the mode can be determined by setting $\partial\rho^{\text{eq}}(x)/\partial x = 0$ (or equivalently $\partial U(x)/\partial x = 0$). In the no-interaction limit, $\alpha_{mw}, \alpha_{wm} \to 0$, with mutation rate μ and intrinsic selection coefficient s_m, the peak of the stationary probability distribution is given by the following relation:

$$x_{\text{mode}}(\mu, s_m) = \frac{-2\mu + s_m + \text{sgn}(s_m)\sqrt{4\mu^2 + s_m^2}}{2s_m}. \tag{12}$$

In the modification of the population by ecological interactions, our specific cases of interest reflect the position of the modal value of the population with respect to the initial modal value of a system without interactions. However, while numerical calculation of the modal value for given interaction coefficients and intrinsic selection is possible (e.g., **Fig. 3**), a general expression for the peak of the distribution with interactions is intractable.

As an alternative analytical approach to gain insight into the effects of game interactions, we examined the selection coefficient $\sigma_m(x)$ from **Eq.** (8) evaluated at the modal frequency (x_{mode}) in the absence of interactions. This can be interpreted as the hypothetical selection effect that would be observed if we were to suddenly turn on interactions in a previously non-interacting system. It provides information about how the system would evolve in response to these interactions and allows us to define the various eco-evolutionary regimes described in the next section. The expression for $\sigma_m(x_{\text{mode}})$ is given by:

$$\sigma_m(x_{\text{mode}}) = \frac{2s_m^2 + s_m(\alpha_{mw} - \alpha_{wm}) + (\text{sgn}(s_m)2\mu - \sqrt{4\mu^2 + s_m^2})(\alpha_{mw} + \alpha_{wm})}{2s_m + \alpha_{wm}(s_m + \sqrt{4\mu^2 + s_m^2} - \text{sgn}(s_m)2\mu)}. \tag{13}$$

In the absence of interactions (α_{mw}, $\alpha_{wm} \to 0$) this reduces to the intrinsic selection coefficient s_m.

Specific conditions on interactions define maintenance, masking, mirroring, and mimicry

Biologically, while intrinsic selection advantages can be present, cells within heterogeneous populations must survive selection under eco-evolutionary dynamics. Taking into account the effects of both ecological and mutational forces, survival of or out-competition by a sub-population may play out in a variety of ways: the maintenance of existing intrinsic selection

	$\sigma > 0$	$\sigma < 0$
Maintenance	$\alpha_{wm} = \frac{\mu\alpha_{mw}}{s_m(1+s_m)}$	$\alpha_{mw} = -\frac{\mu\alpha_{wm}(1+s_m)}{s_m}$
Masking	$\alpha_{wm} = \alpha_{mw} + 2s_m$	$\alpha_{mw} = \alpha_{wm} - 2s_m$
Mirroring	$\alpha_{wm} = -\frac{2s_m}{(1-s_m)} + \frac{2s_m+\alpha_{mw}}{(1-s_m)s_m}\mu$	$\alpha_{mw} = -2s_m - \frac{2s_m-\alpha_{wm}(1-s_m)}{s_m}\mu$
Mimicry	$\alpha_{wm} = -\frac{\sigma}{1+\sigma} + \frac{\mu(\alpha_{mw}-\sigma)}{\sigma(1+\sigma)}$	$\alpha_{mw} = \sigma - \frac{\mu(\sigma+(1+\sigma)\alpha_{wm})}{\sigma}$

Table 1. Surfaces that define the maintenance, masking, mimicry, and mirroring regimes. These regimes are defined by constraints on one interaction coefficient as a function of the other system parameters. Thus each condition is a surface in three (for masking) or four-dimensional space (for the other regimes). In the no mutation limit ($\mu \to 0$) we are able to evaluate whether equivalent regimes exist in deterministic systems.

advantages, the masking of selection differences, or the mimicry of intrinsic selection in its absence. Furthermore, one can also observe mirroring, the complete inversion of the landscape due to interactions. These concepts are of interest when we attempt to interpret the results of co-evolutionary dynamics in the outcomes of experiments.

We hypothesized that the concepts of maintenance, masking, mirroring, and mimicry (as illustrated in **Fig. 1**) are the result of specific relationships between the interaction-dependent selection and intrinsic selection coefficient which are in turn determined by the relationship between the interaction coefficients. For a given interaction selection coefficient $\sigma_m(x_{\text{mode}})$, the relationship between interaction coefficients α_{mw} and α_{wm} can be found by rearranging **Eq.** (13)**.** We use σ to represent $\sigma_m(x_{\text{mode}})$ for brevity. The relation is as follows:

$$\alpha_{wm} = \frac{2s_m(s_m-\sigma) + (s_m + 2\mu - \sqrt{4\mu^2+s_m^2})\alpha_{mw}}{(1+\sigma)(s_m - 2\mu + \sqrt{4\mu^2+s_m^2})}. \tag{14}$$

As described below, we can use this formula to obtain simplified expressions that define the maintenance, masking, and mimicry regimes, summarized in **Table 1**. In each case, the limit $\mu \to 0$ corresponds to these regimes (where possible) that are present in deterministic systems. The graphical representation of these relationships are illustrated for a range of selection (s_m) and mutation (μ) parameters in the Supplementary Information (**Fig. S3**)

The first regime, *maintenance*, is defined where the relative interaction strengths α_{mw}, α_{wm}, and monoculture selection coefficient s_m maintain the same selective advantage as in the absence of interactions, namely $\sigma_m(x_{\text{mode}}) = s_m$. In this context the interaction terms are non-zero but leave the evolutionary outcome unchanged, producing the same modal equilibrium value as if there were no interactions. We call this behavior *maintenance* as interactions maintain the growth rates of the monoculture populations. Maintenance is only possible via the effects of mutations, since when $\mu \to 0$ the regime reduces to the trivial non-interacting case α_{wm}, $\alpha_{mw} = 0$. In the second regime, fitness differences between a wild-type and a mutant in monoculture may be counteracted by interactions when they are grown in co-culture. We call this the *masking* scenario, where intrinsic fitness differences are neutralized by interactions. This is defined by the effective selection coefficient $\sigma_m(x_{\text{mode}}) = 0$ when $s_m \neq 0$. The reverse case is also possible, where wild types and mutants may have a neutral fitness relationship in monoculture, but when grown in co-culture, there is a selective fitness difference. In this case, the interaction coefficients allow for an advantage in the presence of no intrinsic selection differences. We call this scenario *mimicry*. At x_{mode}, we may express this as $\sigma_m(x_{\text{mode}}) = \sigma \neq 0$, a constant, when $s_m = 0$. In the final regime, we consider *mirroring*, whereby the selection difference between the wild-type and mutant fitness seen in monoculture is perfectly inverted. This can be expressed as $\sigma_m(x_{\text{mode}}) = -s_m$, the opposite sign compared to that in monoculture.

To validate the theoretical restrictions (on α_{wm} and α_{mw}) that would result in the modification, masking, or maintenance discussed above we simulated the dynamics of an evolving population with and without the interaction terms (**Fig. 5**). The plots at the top of this figure display the relationships from **Table 1** for each example case. We show boxplots of simulation results, where initial simulations with no interactions ("Selection only") are compared to simulations with added interaction terms for three different intrinsic selection coefficients and two mutation rates.

Each simulation model consists of a population of $1,000$ individuals undergoing mutation and selection and each boxplot represents 50 individual simulations. In each case, the analytical modal values for populations with no interactions and different

intrinsic selection coefficients are marked with dotted lines. For each subplot, along the x axis the strength of interactions (magnitude of α_{mw}) is increased, and the corresponding value of α_{wm} is calculated for each set of simulations from the formulae in **Table 1**. Similar results for expanded parameter ranges are shown in **Figure S4**.

In the *maintenance* case, the no-interaction simulations fall on the theoretical fractions (dotted lines) for the appropriate selection (s_m) as expected. As predicted theoretically, the mean populations in the *maintenance* interaction cases remain centered on the same theoretical value as in the no interactions ("Selection only"). The population means have the same values. Changing ecological interactions maintain the intrinsic selection.

In the *masking* case, the no-interaction simulation means to the left ("Selection Only") agree with those predicted from the selective differences. As predicted theoretically, the mean populations in the *masking* case are all centered on the equal 50:50 split, the theoretical value for the masked (neutral) case. The intrinsic selection difference is masked by ecological interactions.

In the *mirroring* case, the no-interaction cases are aligned with the analytical results expected for the given selective differences. As predicted theoretically, the mean populations in the *mirroring* case all are perfectly reflected and the model value moves to the inverted fraction $(1-x)$ of the population. The selection advantage of one population is inverted by the ecological interaction.

In the *mimicry* case, the theoretical modal values for all simulations with no interactions are at 50% as marked with the purple dotted line. The no-interaction cases are all neutral as expected in the mimicry scenario. As predicted theoretically, the mean populations in the *mimicry* case all lie on the theoretical means for the three selection coefficients.

Strengths of ecological interactions vary and can produce maintenance, masking, and mirroring effects in *in vitro* experiments

To demonstrate how the reformulation of the payoff matrix can allow game theorists and biologists to better understand eco-evolutionary dynamics, we carried out a literature search to identify direct measured payoff matrices or co-culture experiments from which the payoff matrix [17] can be defined (see Methods). The traditional game-space representation of the payoff matrices from the literature is shown in **Fig 6A**. The color represents the publication from which these are derived and each dot is an individual reported measurement of the payoff or growth rates. Numbered experiments represent different payoff results from the same paper and are numbered to highlight specific ordering and positional changes between plots. While this traditional plot is sufficient to determine the proportions of populations at equilibrium, the plot is non-unique with respect to the intrinsic and extrinsic contributions to the payoff matrix. We used our payoff matrix reformulation and examined only published results with sufficient information to determine the magnitudes of selection and interaction effects. [8, 9, 17, 42–45] We create the "interaction-selection" plot, presenting the cell-extrinsic interaction coefficients $(\alpha_{mw}, \alpha_{wm})$, on the axes, divided by the cell-intrinsic selection coefficient s_m. This new "interaction-selection" plot illustrates the direction and intensity of the two interactions terms in a measured payoff matrix. Within this plot, the unit circle (blue) shown in **Fig 6B** represents the boundary between dominance of ecological versus intrinsic selection effects. Within this circle a system's dynamics are dominated by intrinsic fitness differences, outside of the circle they are dominated by ecological effects. We see that this visualization gives us additional information including allowing us to distinguish strong and weak ecological effects relative to selection that may result in very similar equilibrium proportions (i.e. point 1 and 6). This plot allows us to see the relative strengths of individual eco-effects compared to selection. For example, result 7, with large positive $c-a$ value and large negative $b-d$ value in **Fig 6A** lies close to the unit circle in **Fig 6B** . The distribution of values from Deris *et al.* [45] all have strong reported ecological effects (negative, competitive) relative to selection differences. We see that for Farrokhian *et al.*(Pink, 0-4) [8], the relative strength of interactions is higher in 3 than 4 and the sign of the interaction effect on the mutant is reverse in the no-drug condition (0). We note that all bacteria interaction terms lie within [-2,2]. The two most extreme examples of interaction-to-selection ratios $\frac{\alpha_{ij}}{s_j} > 5$ are in cancer models (6, cell line [17] and dark blue, PDX [45] respectively).

We have previously presented the concepts of maintenance and masking to highlight that when ecological interaction effects are present in co-culture, they can reinforce prior assumptions. In assuming that there is an absence of interaction or an absence of intrinsic selection, it is possible to miss potentially confounding biological components underlying a similar net result. To understand to what extent the specific regimes of maintenance, masking, and mirroring may be present in real multi-species systems, we examine the experimental coordinates of the selection and interaction coefficients and their position with respect to the aforementioned theoretical regimes.

Each of the *maintenance*, *masking*, and *mirroring* regimes is defined by a function $a_{wm} = f(s_m, a_{mw}, \mu)$ (**Table 1**). These conditions thus correspond to analytically defined manifolds. The minimum distance of the experimental system from each theoretical regime was calculated as the perpendicular distance from the measured value $[s_m, a_{mw}, a_{wm}]$ to the closest projection of the point onto the surface. These values are shown for each paper and each condition in **Fig 6C**. Multiple systems are seen as approximating maintenance (star), mirroring (circle), and masking (triangle). Mirroring becomes more common in strong selection regimes where $s_m \geq 1$. In **Fig 6D-F** we simulate the eco-evolutionary dynamics of two populations in the highlighted cases. Dynamics are plotted without the interaction components (yellow, red) and then when the interactions are

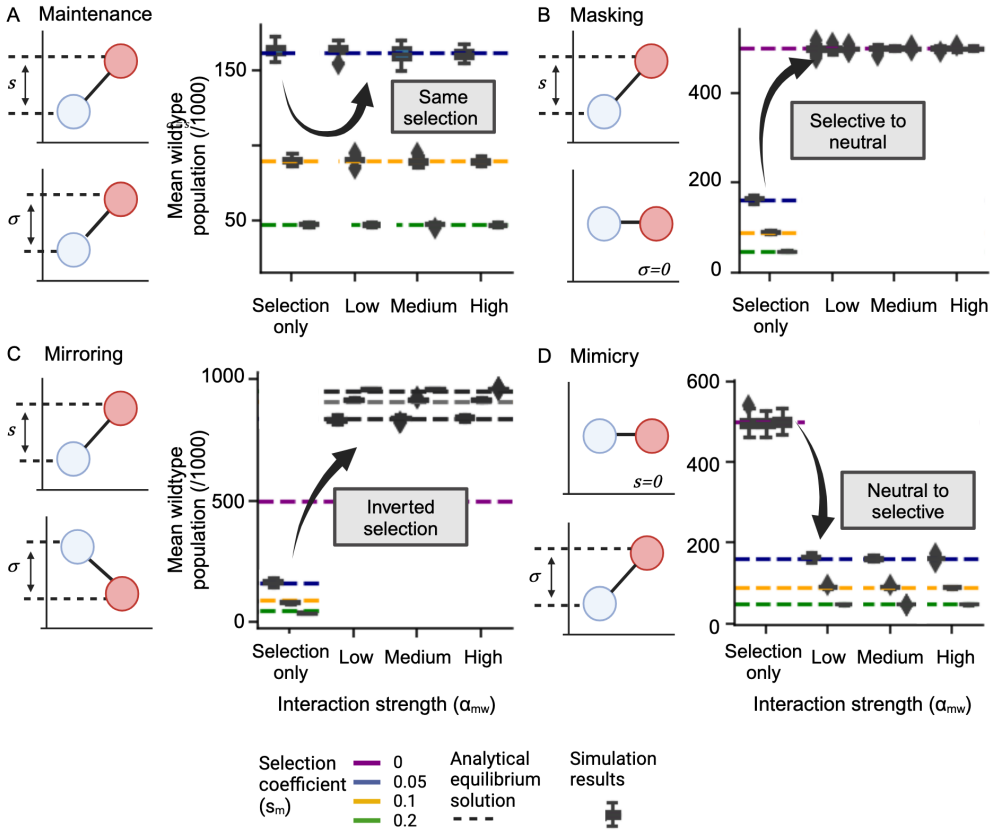

Figure 5. Analytical conditions for Maintenance, Masking, Mirroring, and Mimicry are validated in stochastic simulations and validity is insensitive to initialized selection and interaction strength. Simulations were carried out for each scenario and a genetic population comprising individuals with one of two possible alleles ($N = 1000$), with no interactions (Selection only), and with interactions. Dashed lines represent the theoretical modal value of the wild-type fraction at different intrinsic selection values. For all scenarios, we compare non-ecological simulations with interaction coefficients $\rightarrow 0$ (Selection only), with simulations with increasing strength of ecological interactions. Added ecological interactions have the ratios defined in **Table 1**. **(A)** For maintenance, the simulations maintain the same mean wild-type fraction as in the case with no interactions. **(B)** For the masking scenario, the initial modal fraction of the wild type at each selection coefficient is not 50%. When interactions are introduced, the modal population changes to 50%, the equivalent of no selection. **(C)** In the case of mirroring, the population fraction for three different selection coefficient and interaction coefficient strengths all align with the analytical model. **(D)** In the mimicry case, the initial population is 50% as the mutant population has no intrinsic selection coefficient. With the mimicry interactions, we recapitulate the specific selection coefficients in each case. All simulations show agreement with our theoretical conditions across different strengths of α_{mw} and different values of s and μ. Mean population values are averaged over 3000 generations after an initial 1000 generations. Each box plot represents the distribution of 50 independent simulations. Initial conditions for the simulations were a 50:50 wild-type (0) and mutant (1) population.

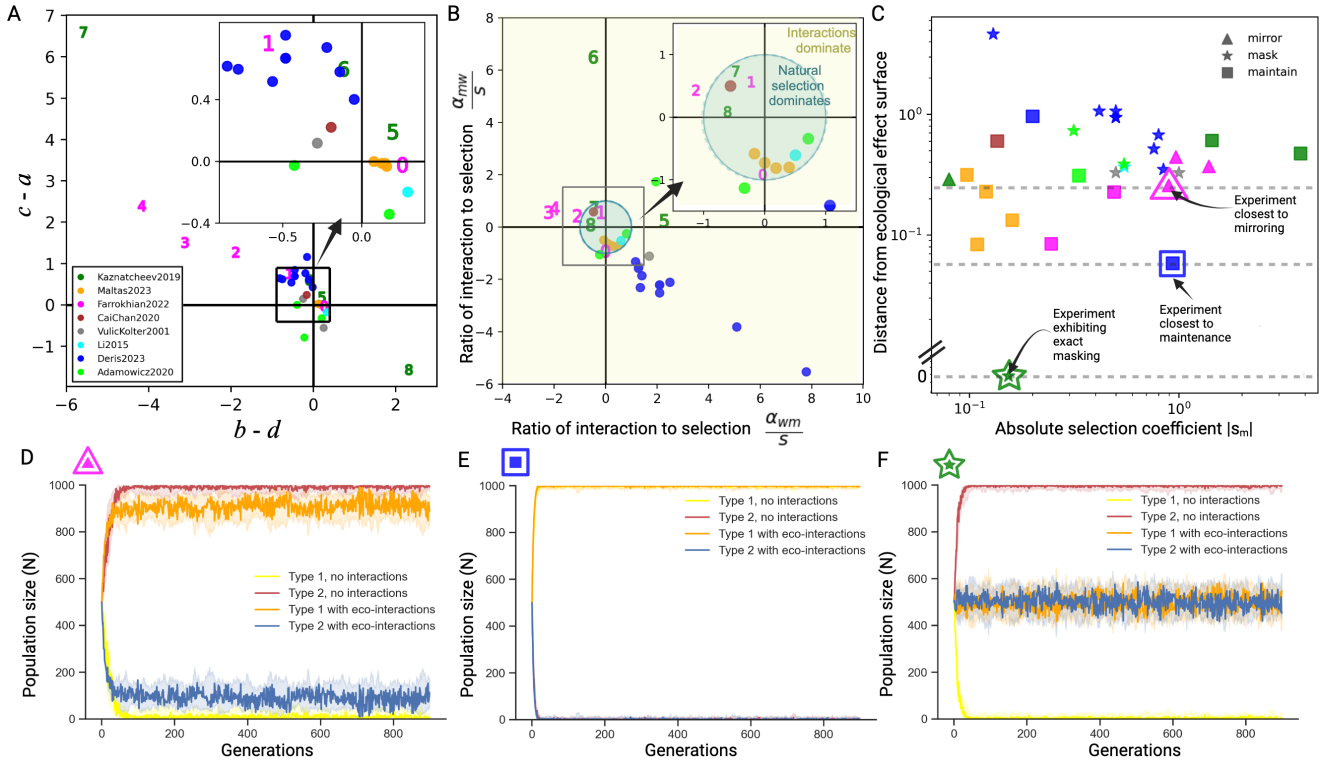

Figure 6. Interaction strengths decoupled from intrinsic selection shows differential dominance of ecology and experimental evidence of potentially misleading ecologically dominated regimes. Games, colored by publication reference, as measured in published experiments. Farrohkian (0-4) and Kaznetcheev (5-9) experiments are numbered for communication and illustration purposes. **A)** Experimental measured games are displayed in "traditional" relative growth rate encoded game space. Inset plot expands area for visibility. **B)** Interaction-selection plot. Distribution of published experimental interaction values relative to intrinsic selection. The unit circle (blue) is the boundary representing equal magnitudes of ecological and intrinsic selection. Experiments inside the circle are dominated by intrinsic selection and those outside the circle are dominated by interaction effects. **C)** Distances of published payoff composition from theoretical maintenance, masking, and mirroring surfaces are shown. The experimental payoff matrices closest to masking (green star), maintenance (blue square) and mirroring (pink triangle) are highlighted. **D-F)** Simulations using the highlighted published experiments in **(C)** illustrate the time-dependent eco-evolutionary dynamics. The population dynamics are simulated for the three experiments most mirror-like, maintenance-like, and masking-like.

present (orange, blue). We see that while the Farrokhian experiment in **D** still inverts selection, it deviates more from perfect mirroring, particularly in contrast to the maintenance and masking dynamics clearly seen in **E** and **F**.

For these systems, we approximated a fixed $\mu = 0.001 \ll 1$. *Mimicry* was excluded from this analysis because although the presentation of a selective advantage from purely ecological means is an interesting evolutionary mode/adaptation, testing for it requires prior knowledge of the otherwise arbitrary "target" selection coefficient σ.

Key details about the publications and data points are shown in **Table 2** and the full data table is included in the Supplementary Information (**Table S2**). For each publication, either the directly reported payoff matrix or a payoff derived from the published growth rates in monoculture and coculture were used (see **Methods**). It is worth noting that the Cai et al. paper [44] uses metabolic models to determine a numerical payoff matrix. In Deris *et al.* [45], the calculations of the payoff matrices are for ten individual patient-derived xenograft (PDX)-mouse models. However, the tumor samples in this experiment originate from the same patient and therefore are biological replicates. Furthermore, calculations of these payoff matrices in this publication are done in such a way that restricts the payoff matrices to competitive interactions only.

Discussion

The approach of the cell biologist often requires the isolation of microscopic populations to understand their properties. Ecologists, however, focus primarily on the interactions of populations on a macroscopic scale. While both agree that interactions between populations can have implications, they work under assumptions often at extreme ends of the spectrum. We focus on the eco-evolutionary regime in which both intrinsic fitness and ecological interactions play a role.

These ideas find importance in the future of human diseases, where *in vitro* work has also solidified the existence of cell-cell interactions and their importance. A range of novel "game assays" have also begun to quantify these interactions between cells

Table 2. Experimental payoff systems and associated papers. Results from the following papers were used to derive corresponding selection and interaction coefficients in their payoff matrices. *Li *et al.* found that the relationship between frequency and fitness was non-linear, but the linear assumption in our model was used for linear payoff matrix estimation from their data.

Author	Year	System	Variable	Number of matrices
Vulic and Kolter [42]	2001	Bacteria	Mutation	1
Li *et al.** [15]	2015	Bacteria	Species	1
Kaznatcheev *et al.* [17]	2019	Cancer	Drug+CAFs	4
Adamowicz *et al.* [43]	2020	Bacteria	Mutation	3
Cai *et al.* [44]	2020	In-silico	Metabolic simulation	1
Farrokhian *et al.* [8]	2020	Cancer	Mutation, Drug	5
Deris *et al.* [45]	2023	Cancer	PDX Replicates	4
Maltas *et al.* [9]	2024	Cancer	Mutation, Drug	4

in culture. [17] Understanding how to bridge the gap between the co-evolution in complex disease and the theory is critical to future treatment approaches. We use ecology and game theoretical concepts to model and explore the possible impacts of these interactions as they become increasingly important in the disease and cell-biology perspectives. [46]

Our work builds on existing experimental and mathematical descriptions of eco-evolutionary dynamics. [8, 30–32] To bridge the gap between theory and biology, we acknowledge that in laboratory experiments where cell lines are typically isolated, monoculture fitnesses of cells are typically the most well-studied property. By reframing the game matrix such that the interactions and monoculture fitnesses are separated, we come to a form that can both be interpreted within the Fokker-Planck formalism but also better understood from the perspective of evolutionary population dynamics in cell lines.

We highlight the critical nature of game interactions from an experimental perspective, demonstrating exactly how the presence of game interactions in addition to the underlying genotypic fitness difference has the potential to modify the evolutionary outcome of an evolving population to any desired outcome. We derive a general expression for the equilibrium distribution of a population obeying the Fokker-Planck equation with selection and arbitrary interactions. We reveal, using analytical theory and simulations, the potential impacts of game interactions and their ability to completely alter evolutionary dynamics. We find the critical boundaries at which these game dynamics either maintain a population at the originally fitter genotype (maintenance), move a population from the fixation of the fitter genotype in monoculture to the fixation of the other (mirroring), promote fixation of a population in the absence of intrinsic selection differences (mimicry), or even promote the heterogeneity of a population by leveling the playing field (masking).

We find that the ability for interactions in co-culture to maintain the same relative monoculture fitness advantage depends on the mutation rate between the two alleles. Additionally, the interaction strengths required to mask selection and promote neutral evolution and co-existence are independent of mutation rate. Finally, we find that equally fit populations in monoculture can interact in ways in co-culture to perfectly mimic the composition resulting from the co-evolution of genotypically distinct populations. This result means that the measured outcome of any mixed population, such as tumor cells, must be interpreted with caution.

Even in our simplified case, the (observed) fitness of the cells in question can be significantly altered by moderate cell-cell interactions. We posit that growth dynamics in mixed populations may readily bear little resemblance to monoculture growth rates and that initial seeding (eg. experimental or metastatic) ratios may have strong impacts on resultant dynamics. Without specific techniques designed to robustly assay frequency-dependent game interactions, [8, 17] the magnitude and impact of cell-extrinsic interactions cannot be quantified. These effects have widespread potential ramifications, for example when assaying chemotherapeutic drugs in isolated cell lines, when developing cancer cell lines *ex vivo*, and when interpreting evidence for neutral evolution in tumors. [47–51] We reviewed the experimental literature for payoff matrices, bringing together a range of data in a single framework via our novel interaction-selection plot examining interaction effects. We also demonstrated the relevance of these potentially counter-intuitive eco-evolutionary modes in published data. Further work aimed at outlining to what extent these modes of eco-evolution can be seen in systems with logistic growth and carrying capacities, typically modeled using Lotka-Volterra competition models, [5] would allow further application of these concepts to additional experiment types.

The limitations of our work include limitation to a two-genotype, non-spatial system. We do not cover the mechanistic aspects of these interactions or include environmental parameters or interaction effects that vary with time. We also assume linearity of the frequency-dependent interactions, an assumption that likely does not hold true across all systems. Additionally, in order to analyze and discuss previously published results from the literature, simplifying assumptions were made about mutation rates. Although in the published results we see several relatively strong ecological effects, the results shown are not exhaustive. Although interactions here are evident, there is likely a positive bias in the literature toward the publication of experimental results where ecological interactions are present.

Whilst our work focused on the modal value of the equilibrium distribution after a long period, the varying higher-order properties of the Fokker-Planck distributions suggest that systems with games may also have altered evolutionary dynamics over time. This has been noted in previous work, [26] where Kaznatcheev demonstrated that evolution is, in some cases, accelerated by game interactions. Future work could derive explicit expressions for signatures of game dynamics that are encapsulated in the higher-order properties (standard deviation, skew) of the equilibrium solutions. Identifying these factors may be critical in interpreting the existence and strength of cell-cell interactions in experimental populations. Decomposition of the payoff matrix provides a biologically meaningful formulation of the payoff matrix and the ability to independently modify the cell-intrinsic and cell-extrinsic contributions to the growth rate. In addition to supplying a new modeling paradigm and analytical solution in the case of added noise, this formalism provides an ideal starting point for the integration of existing pharmacokinetic understanding into game theoretical models. This model framework also more readily permits the integrated modeling of evolutionary therapy. These frameworks can assist calculations for optimal stochastic control and adaptive therapy in the presence of experimentally motivated drug and micro-environmental-dependent ecological cell interactions. [8, 52–55]

Methods

Simulations

Using Python (version 3.11.5), we developed a stochastic Wright-Fisher type population model with discrete non-overlapping generations modified from Bedford *et al.* [56] Creating a two-genotype model, we incorporated generational sampling that was weighted by frequency in ratios given by the coefficients of a payoff matrix. We used this to observe the simulated evolutionary trajectories and stationary distribution before and after the addition of game interactions of different strengths. In particular, we asked whether our simulation results are consistent with game interactions designed to maintain, mimic, or mask the expected evolutionary outcome that would be based on monoculture fitness alone.

The simulations (parameter ranges in **Table 3**), involved a constant population of size N comprised of two species, denoted wild-type ('0') and mutant ('1'), undergoing mutation (rate μ) and selection at each generation. The sampling frequency of each population was based on the frequency-dependent fitness of each population calculated at each generation. The constant population size N, mutation rate μ, and mutant advantage s_m were all fixed for each simulation. When random net payoff matrix values or interaction strengths (α_{ij}) were required, they were generated using a random uniform distribution within a given range. In each simulation, populations were allowed to evolve from an initial fraction x_i for 1000 generations, at which point the population fraction from each simulation was extracted.

Table 3. Methodological parameter values and ranges for the frequency-dependent Wright-Fisher model

Parameter	Symbol	Value(s)
Mutation rate (per generation)	μ	1×10^{-2}, 1×10^{-3}
Population size	N	100-10000
Generations	-	500-1000
Initial fraction (i)	x_i	(0,1)
Intrinsic selection	s	(0,0.5)
Interaction effect of i on j	α_{ij}	(-1,1)

Intrinsic selection and extrinsic interaction values from the literature

We found coculture experiments published in the literature, [8, 9, 17, 42, 43, 45] and converted them to normalized and decoupled payoff matrices. Decoupled payoff matrices are expressed in terms of both intrinsic selection and ecological growth rate effects (see **Eq. 3**). Our search was restricted to published results that explicitly reported experimentally derived payoff matrices [8, 9, 17]or publications with experimental growth rates for populations in both mono- and co-culture. Details of the publications, system or experiment type, and number of payoff matrices are shown in **Table S2**.

To calculate the payoff matrix and thus interaction values and selection from mono- and co-culture growth rate information, it is possible to construct an ecological interaction (*growth-frequency*) plot for both populations (**Fig. S5**) from which the intersections (payoff values) can be inferred. With the payoff matrix generated, intrinsic and extrinsic growth rate modifiers can be calculated.

Distance of experiments from maintenance, masking, and mirroring surfaces

The maintenance, masking, and mirroring surfaces were defined in **Table 1**. To calculate the proximity of the published experiments' payoff values to the theoretical manifolds representing maintenance, masking, and mirroring (see GitHub for code)

we used Python to carry out numerical optimization. A small mutation rate was assumed and set at 0.001 for experimentally derived distance calculations.

The dimensionless Euclidean distance between two points was calculated and minimized with respect to points on the surface to approximate the distance of the measured point from the respective manifold. Numerical optimization (numPy) was used to find the shortest distance between the measured value, $(s_m^{exp}, \alpha_{wm}^{exp}, \alpha_{wm}^{exp})$ and points on the surfaces defined for maintenance and mirroring. A Euclidean distance function was minimized subject to this surface constraint. The optimized point is the projection of the original point onto the surface. Then the distance (d_{min}) between the experimental point and its projection is calculated numerically. An illustration of this idea in less than four dimensions is in **Figure S6**.

Acknowledgments

We acknowledge Theory Division members for their insight. JGS thanks the NIH for its support through NIH R37CA244613 and NIH U01CA280829, its Loan Repayment Program, and the Paul Calabresi Career Development Award for Clinical Oncology (NIH K12CA076917). DT thanks the Research Council of Norway 325628/IAR (DST).

Code and data availability

All of the Mathematica and Python scripts in this project can be found on GitHub at;
https://github.com/rbarkerclarke/GamesModifyEvolution. The processed previously published experimental data is available in the supplementary files and the same repository.

References

1. Scott, J. & Marusyk, A. Somatic clonal evolution: A selection-centric perspective. *Biochimica et Biophys. Acta (BBA) - Rev. on Cancer* **1867**, 139–150, DOI: 10.1016/j.bbcan.2017.01.006 (2017).

2. Schaper, S., Johnston, I. G. & Louis, A. A. Epistasis can lead to fragmented neutral spaces and contingency in evolution. *Proc. R. Soc. B.* **279**, 1777–1783, DOI: 10.1098/rspb.2011.2183 (2012).

3. Foo, J. & Michor, F. Evolution of acquired resistance to anti-cancer therapy. *J. theoretical biology* **355**, 10–20 (2014).

4. Volterra, V. Fluctuations in the abundance of a species considered mathematically. *Nature* **118**, 558–560 (1926).

5. Bomze, I. M. Lotka-volterra equation and replicator dynamics: a two-dimensional classification. *Biol. cybernetics* **48**, 201–211 (1983).

6. Schuster, P. & Sigmund, K. Replicator dynamics. *J. theoretical biology* **100**, 533–538 (1983).

7. Hofbauer, J. & Sigmund, K. *Evolutionary games and population dynamics* (Cambridge University Press, 1998).

8. Farrokhian, N. *et al.* Measuring competitive exclusion in non–small cell lung cancer. *Sci. Adv.* **8**, eabm7212 (2022).

9. Maltas, J. *et al.* Frequency-dependent ecological interactions increase the prevalence, and shape the distribution, of pre-existing drug resistance. *in press at PRX Life* DOI: 10.1101/2023.03.16.533001 (2024).

10. Haven, J. *et al.* Pervasive Recombination and Sympatric Genome Diversification Driven by Frequency-Dependent Selection in Borrelia burgdorferi, the Lyme Disease Bacterium. *Genetics* **189**, 951–966, DOI: 10.1534/genetics.111.130773 (2011).

11. Kazancıoğlu, E. & Arnqvist, G. The maintenance of mitochondrial genetic variation by negative frequency-dependent selection. *Ecol. Lett.* **17**, 22–27, DOI: 10.1111/ele.12195 (2014).

12. Marusyk, A. *et al.* Non-cell-autonomous driving of tumour growth supports sub-clonal heterogeneity. *Nature* **514**, 54–58 (2014).

13. Maddamsetti, R., Lenski, R. E. & Barrick, J. E. Adaptation, Clonal Interference, and Frequency-Dependent Interactions in a Long-Term Evolution Experiment with Escherichia coli. *Genetics* **200**, 619–631, DOI: 10.1534/genetics.115.176677 (2015).

14. Sherratt, A. E. T. N. & Whitlock, E. M. C. Frequency Dependence and Cooperation: Theory and a Test with Bacteria. *Am. Nat.* (2015).

15. Li, X.-Y. *et al.* Which games are growing bacterial populations playing? *J. The Royal Soc. Interface* **12**, 20150121 (2015).

16. Harmand, N., Federico, V., Hindré, T. & Lenormand, T. Nonlinear frequency-dependent selection promotes long-term coexistence between bacteria species. *Ecol. Lett.* **22**, 1192–1202, DOI: 10.1111/ele.13276 (2019).

17. Kaznatcheev, A., Peacock, J., Basanta, D., Marusyk, A. & Scott, J. G. Fibroblasts and alectinib switch the evolutionary games played by non-small cell lung cancer, journal = Nat. Ecol. Evol., volume = 3, pages = 450–456, year = 2019, month = Mar, issn = 2397-334X, publisher = Nature Publishing Group, doi = 10.1038/s41559-018-0768-z.

18. Basanta, D., Simon, M., Hatzikirou, H. & Deutsch, A. Evolutionary game theory elucidates the role of glycolysis in glioma progression and invasion. *Cell proliferation* **41**, 980–987 (2008).

19. Basanta, D., Hatzikirou, H. & Deutsch, A. Studying the emergence of invasiveness in tumours using game theory. *The Eur. Phys. J. B* **63**, 393–397 (2008).

20. Basanta, D. *et al.* Investigating prostate cancer tumour–stroma interactions: clinical and biological insights from an evolutionary game. *Br. journal cancer* **106**, 174–181 (2012).

21. Archetti, M. Evolutionary game theory of growth factor production: implications for tumour heterogeneity and resistance to therapies. *Br. J. Cancer* **109**, 1056, DOI: 10.1038/bjc.2013.336 (2013).

22. Mirzaev, I., Williamson, D. F. & Scott, J. G.. egtplot: A python package for three-strategy evolutionary games. *J. Open Source Softw.* **3**, 735 (2018).

23. Hurlbut, E., Ortega, E., Erovenko, I. V. & Rowell, J. T. Game theoretical model of cancer dynamics with four cell phenotypes. *Games* **9**, 61 (2018).

24. Gluzman, M., Scott, J. G. & Vladimirsky, A. Optimizing adaptive cancer therapy: dynamic programming and evolutionary game theory. *Proc. Royal Soc. B* **287**, 20192454 (2020).

25. Taylor, A. E. P. D. & Day, E. T. Frequency-Dependent Selection Can Lead to Evolution of High Mutation Rates. *Am. Nat.* (2015).

26. Kaznatcheev, A. Evolution is exponentially more powerful with frequency-dependent selection. bioRxiv [Preprint] 2020.05.03.075069 (2021). 2020.05.03.075069.

27. Imhof, L. A. & Nowak, M. A. Evolutionary game dynamics in a Wright-Fisher process. *J. Math. Biol.* **52**, 667–681, DOI: 10.1007/s00285-005-0369-8 (2006).

28. Chalub, F. A. C. C. & Souza, M. O. The frequency-dependent Wright–Fisher model: diffusive and non-diffusive approximations. *J. Math. Biol.* **68**, 1089–1133, DOI: 10.1007/s00285-013-0657-7 (2014).

29. Iram, S. *et al.* Controlling the speed and trajectory of evolution with counterdiabatic driving. *Nat. Phys.* **17**, 135–142 (2021).

30. Traulsen, A., Claussen, J. C. & Hauert, C. Coevolutionary dynamics: from finite to infinite populations. *Phys. review letters* **95**, 238701 (2005).

31. Traulsen, A., Claussen, J. C. & Hauert, C. Coevolutionary dynamics in large, but finite populations. *Phys. Rev. E* **74**, 011901 (2006).

32. Altrock, P. M. & Traulsen, A. Deterministic evolutionary game dynamics in finite populations. *Phys. Rev. E* **80**, 011909 (2009).

33. Taylor, P. D. & Jonker, L. B. Evolutionary stable strategies and game dynamics. *Math. biosciences* **40**, 145–156 (1978).

34. Harley, C. B. Learning the evolutionarily stable strategy. *J. theoretical biology* **89**, 611–633 (1981).

35. Fokker, A. D. Die mittlere energie rotierender elektrischer dipole im strahlungsfeld. *Annalen der Physik* **348**, 810–820 (1914).

36. Planck, V. "On a theorem of statistical dynamics and its extension in quantum theory". *session reports* (1917).

37. Woo, H.-J. Analytical theory of the nonequilibrium spatial distribution of rna polymerase translocations. *Phys. Rev. E* **74**, 011907 (2006).

38. Polotto, F., Drigo Filho, E., Chahine, J. & de Oliveira, R. J. Supersymmetric quantum mechanics method for the fokker–planck equation with applications to protein folding dynamics. *Phys. A: Stat. Mech. its Appl.* **493**, 286–300 (2018).

39. Degond, P., Herda, M. & Mirrahimi, S. A Fokker-Planck approach to the study of robustness in gene expression. *arXiv preprint arXiv:2006.14985* (2020).

40. Baughman, G. & Sharma, P. Entropic analysis of protein oscillations through Langevin equations & Fokker-Planck equations. *J. Human, Earth, Futur.* **3**, 56–70 (2022).

41. Kimura, M. *et al. Stochastic processes and distribution of gene frequencies under natural selection* (Citeseer, 1954).

42. Vulić, M. & Kolter, R. Evolutionary cheating in escherichia coli stationary phase cultures. *Genetics* **158**, 519–526 (2001).

43. Adamowicz, E. M., Muza, M., Chacón, J. M. & Harcombe, W. R. Cross-feeding modulates the rate and mechanism of antibiotic resistance evolution in a model microbial community of escherichia coli and salmonella enterica. *PLoS pathogens* **16**, e1008700 (2020).

44. Cai, J., Tan, T. & Chan, S. H. Predicting nash equilibria for microbial metabolic interactions. *Bioinformatics* **36**, 5649–5655 (2020).

45. Deris, A. & Sohrabi-Haghighat, M. Analysis of cancerous tumor growth by the competitive model based on the evolutionary game theory. *Int. J. Nonlinear Analysis Appl.* **14**, 1903–1910 (2023).

46. Janiszewska, M. *et al.* Subclonal cooperation drives metastasis by modulating local and systemic immune microenvironments. *Nat. cell biology* **21**, 879–888 (2019).

47. Sottoriva, A. *et al.* A big bang model of human colorectal tumor growth. *Nat. genetics* **47**, 209–216 (2015).

48. Williams, M. J., Werner, B., Barnes, C. P., Graham, T. A. & Sottoriva, A. Identification of neutral tumor evolution across cancer types. *Nat. genetics* **48**, 238–244 (2016).

49. Davis, A., Gao, R. & Navin, N. Tumor evolution: Linear, branching, neutral or punctuated? *Biochimica et Biophys. Acta (BBA)-Reviews on Cancer* **1867**, 151–161 (2017).

50. McDonald, T. O., Chakrabarti, S. & Michor, F. Currently available bulk sequencing data do not necessarily support a model of neutral tumor evolution. *Nat. genetics* **50**, 1620–1623 (2018).

51. Tung, H.-R. & Durrett, R. Signatures of neutral evolution in exponentially growing tumors: A theoretical perspective. *PLOS Comput. Biol.* **17**, e1008701 (2021).

52. Yoon, N., Vander Velde, R., Marusyk, A. & Scott, Jacob G. Optimal therapy scheduling based on a pair of collaterally sensitive drugs. *Bull. mathematical biology* **80**, 1776–1809 (2018).

53. Cunningham, J. *et al.* Optimal control to reach eco-evolutionary stability in metastatic castrate-resistant prostate cancer. *PLOS ONE* **15**, 1–24, DOI: 10.1371/journal.pone.0243386 (2020).

54. Lin-Rahardja, K., Weaver, D. T., Scarborough, J. A. & Scott, J. G. Evolution-informed strategies for combating drug resistance in cancer. *Int. J. Mol. Sci.* **24**, 6738 (2023).

55. Wang, M., Scott, J. G. & Vladimirsky, A. Threshold-awareness in adaptive cancer therapy, Threshold-awareness in adaptive cancer therapy, bioRxiv [Preprint], (2024).

56. Bedford, T., Cobey, S. & Pascual, M. Strength and tempo of selection revealed in viral gene genealogies. *BMC evolutionary biology* **11**, 1–16 (2011).